Experimental Astronomy
https://doi.org/10.1007/s10686-018-9616-z

ORIGINAL ARTICLE

# In-flight measurement of Planck telescope emissivity

**F. Cuttaia[1] · L. Terenzi[1] · G. Morgante[1] · M. Sandri[1] · F. Villa[1] · A. De Rosa[1] · E. Franceschi[1] · M. Frailis[2] · S. Galeotta[2] · A. Gregorio[2] · P. Delannoy[3] · S. Foley[3] · B. Gandolfo[3] · A. Neto[3] · C. Watson[3] · F. Pajot[4] · M. Bersanelli[5] · R. C. Butler[1] · N. Mandolesi[1,6] · A. Mennella[5] · J. Tauber[7] · A. Zacchei[2]**

Received: 26 January 2018 / Accepted: 26 November 2018 /


## Abstract

The Planck satellite in orbit mission ended in October 2013. Between the end of Low Frequency Instrument (LFI) routine mission operations and the satellite decommissioning, a dedicated test was also performed to measure the Planck telescope emissivity. The scope of the test was twofold: i) to provide, for the first time in flight, a direct measure of the telescope emissivity; and ii) to evaluate the possible degradation of the emissivity by comparing data taken in flight at the end of mission with those taken during the ground telescope characterization. The emissivity was determined by heating the Planck telescope and disentangling the system temperature excess measured by the LFI radiometers. Results show End of Life (EOL) performance in good agreement with the results from the ground optical tests and from *in-flight* indirect estimations measured during the Commissioning and Performance Verification (CPV) phase. Methods and results are presented and discussed.

**Keywords** Planck satellite · Telescope · Emissivity · Reflection loss · CMB · Cosmic microwave background · Space instrumentation · Microwaves · LNA

✉ F. Cuttaia
francesco.cuttaia@inaf.it

1 INAF, Osservatorio di Astrofisica e Scienza dello Spazio di Bologna, Via Gobetti 101, 40129, Bologna, Italy

2 INAF, Osservatorio Astronomico di Trieste, Via G.B. Tiepolo 11, 34143, Trieste, Italy

3 Mission Operations Centre (MOC), ESA/European Space Operations Centre, Robert-Bosch-Str. 5, 64293 Darmstadt, Germany

4 Institut de Recherche en Astrophysique et Planetologie 9, avenue du Colonel Roche - BP 44346, 31028 Toulouse cedex 4, France

5 Dip. di Fisica, Universita degli Studi di Milano, Via Celoria 16, 20133, Milano, Italy

6 Dip. di Fisica, Universita degli Studi di Ferrara, Via Saragat 1, 44122, Ferrara, Italy

7 Science Directorate, European Space Agency, Keplerlaan 1, 2201AZ Norrdwijk, The Netherlands

## 1 Introduction

The Planck satellite [1, 2] was launched together with the Herschel spacecraft on an Ariane 5 from Europe's spaceport in Kourou, French Guyana, on 14 May 2009. The two satellites were injected into an orbit around the Sun-Earth Lagrange point $L_2$. The duration of the nominal Planck mission was 15,5 months. Nevertheless, Planck operated continuously for 1623 days, until 23 October 2013, with the Low Frequency Instrument (LFI). The High Frequency Instrument (HFI) [3] operated until 13 January 2012, when the supply of $^3$He needed to cool the HFI bolometers to 0.1 K ran out. However, the HFI's He Joule-Thomson cooler [5] continued to operate normally to support the LFI pseudocorrelation radiometers [4] with the required thermal reference at $\sim$ 4K [6] until mission end.

The Planck de-orbiting started on 14 August 2013, when the first manoeuvre for the spacecraft departure from L2 was performed: this phase lasted until October 9th (final de-orbiting manoeuvre).

In the period between October 4th and October 21st, the LFI functionality at End of Life (EOL) was verified: some tests, already performed during the CPV phase [7] or during the ground calibration tests [9–11], were repeated. New additional tests were also performed to verify or better characterize other features revealed during the mission.

In particular, the procedure named Telescope Loss Test (TLT) was run: it was aimed at measuring the Planck telescope emissivity [12] at the LFI frequencies at EOL, by operating the de-contamination heaters located on the primary and the secondary mirrors. This test was not foreseen at the beginning of the Planck mission and was decided upon only during the planning of Planck EOL phase, taking advantage of the LFI radiometers sensitivity [14] and of our improved knowledge of the LFI properties and of the systematic effects over the mission [13, 15].

The test consisted in heating the primary and secondary mirrors by a few Kelvin ($\sim$ 4 K) and then measuring the power excess measured by the LFI pseudocorrelation radiometers. The underlying basic assumption was that the measured excess would be mostly proportional to the telescope reflection loss (emissivity), provided that the other possible effects affecting the radiometric response were known and kept under control.

The TLT procedure was successfully run on 7 October 2013. Such a test was never performed before on a microwave space telescope: the high LFI instrumental sensitivity, a very good knowledge of systematic effects and the Planck Mission Operation Center (MOC) ability in controlling the telescope thermal response were the key ingredients of its success.

## 2 The Planck telescope

The Planck telescope was designed to comply with the following high level optomechanical requirements:

– wide frequency coverage: about two decades, from 25 GHz to 1 THz;

**Fig. 1** the Planck Satellite, on its mounting fixture (MGSE), during the ground tests. The telescope (primary mirror) and the thermal baffle are visible in the foreground

– 100 squared degrees of field of view, wide focal region (400 X 600 mm);
– cryogenic operational environment between 40 and 65 K.

The telescope optical layout was based on a dual reflector off-axis Gregorian design (Fig. 1). Both the primary and secondary mirrors were elliptical in shape. The size of the primary mirror rim was 1.9 X 1.5 meters; the rim of the secondary mirror was nearly circular with a diameter of about 1 meter.

The overall focal ratio was 1.1, and the projected aperture was circular with a diameter of 1.5 meters. The telescope field of view was $\pm 5°$ centred on the line of sight (LOS), which was tilted at about 3.7° relative to the main reflector axis, and

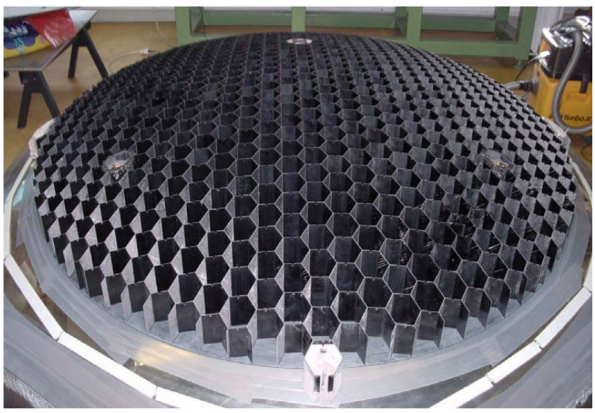

**Fig. 2** Primary Reflector: milled core

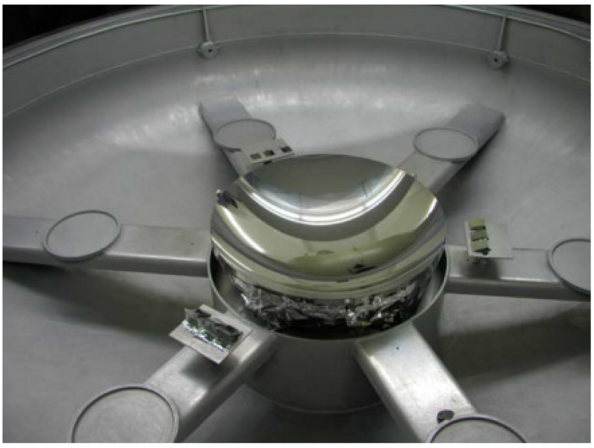

**Fig. 3** Secondary reflector: reflective coating

formed an angle of 85° with the satellite spin axis, which was typically oriented in the anti-Sun direction during the survey.

The Gregorian off-axis configuration ensured a small overall focal ratio (and thus small feeds), an unobstructed field of view, and low diffraction effects from the secondary reflector and struts.

The core of the primary and secondary mirrors was fabricated using Carbon Fiber Reinforced Plastic (CFRP) honeycomb sandwich technology (Fig. 2). The facesheets underwent reflective coating (Fig. 3), following a procedure developed by EADS Astrium, consisting of three layers: 15 nm NiCr as adhesion layer, 550 nm Aluminium as reflective layer, $\sim 30$ nm PLASIL as protection layer [20].

This design was chosen to satisfy the requirements of low mass ( $\leq 120$ Kg including struts and supports), high stiffness, high dimensional accuracy, and low thermal expansion coefficient. Further details on the Planck optical system can be found in [5] and in [21].

## 3 The telescope loss test

The TLT started on 7 October 2013 at 19:25:00 UTC, when *anti-contamination* heating was activated through heaters placed on the primary (PR) and secondary (SR) reflectors. The heaters were operated adapting to the test, in a cyclic fashion, the algorithm that was originally designed for de-contaminating the reflectors during the early launch phases.

Temperatures for decontamination were monitored in real time by three dedicated sensors for each of the Planck reflectors (the three adjacent sensors in line in Figs. 4 and 5, while temperatures used for analysis are measured with a better resolution (about 0.25 K instead of 0.5 K) by two pairs of nominal and redundant sensors (the four symmetrically distributed sensors in Figs. 4 and 5), for each reflector.

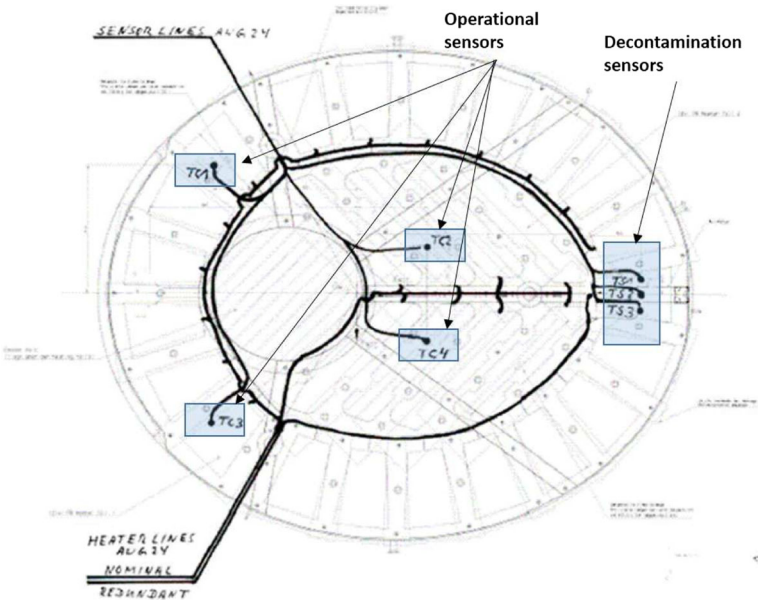


**Fig. 4** Primary reflector: heaters harness and temperature sensors location scheme

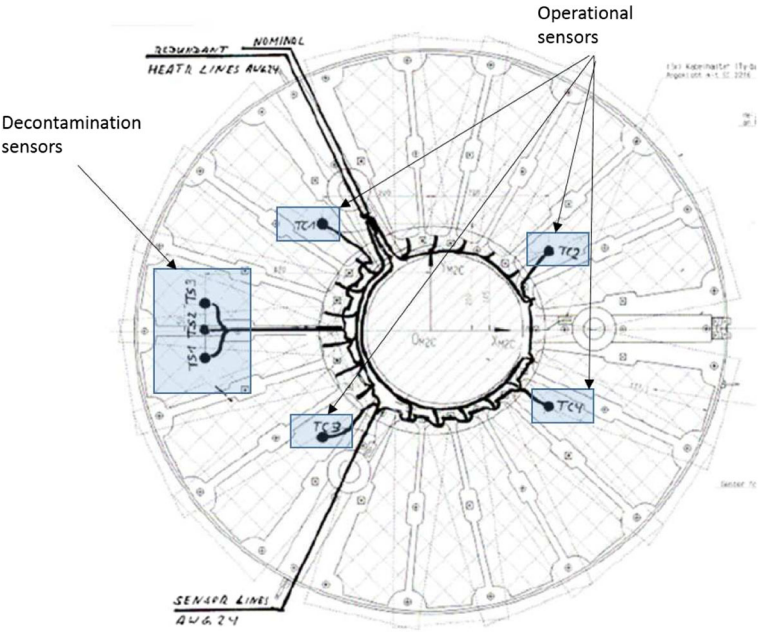


**Fig. 5** econdary Reflector: heaters harness and temperature sensors location scheme

On the basis of the emissivity measured during the ground tests, a minimum temperature change of 2 K was required to unambiguously characterize the in-flight emissivity, expected lower than 0.0006 in the LFI frequency range. Nevertheless, the overall decontamination procedure was able to increase the temperature of the PR and SR by roughly 4 K (averaged over the corresponding monitoring sensors), while the temperatures remained quite stable for the last 90 minutes of the test.

Finally, both reflectors started to cooldown at a rate of less than 1 K in 12 hours.

Temperature profiles of PR and SR, caused by anti-contamination heaters activation and de-activation, are respectively shown in Figs. 12 and in Fig. 13.

## 4 Emissivity characterization

The emissivity plays a crucial role in microwave telescopes, even more in spinning telescopes like Planck. Actually, the black-body thermal emission from the telescope is the cause of a higher system temperature; moreover, thermal fluctuations of the telescope can mimic the effect of changes in sky emission, which is critical especially at fluctuation frequencies near the satellite spin frequency. For this reason the telescope emissivity was required, at beginning of life (BOL), to be lower than 0.6%.

The telescope emissivity was expected to change during the mission due to UV irradiation and micrometeoroid impact, especially at the HFI frequencies.

The emissivity was estimated on ground, by measuring the reflection loss of several samples from the Herschel telescope [16]. However, due to non-negligible differences between the Herschel and Planck telescopes, more accurate tests, based on a high-quality open Fabry-Perot resonator, were performed in 2008, directly on same Planck telescope samples, between 100 and 380 GHz [18], at the Institute of Applied Physics of the Russian Academy of Sciences (IAP RAS). Measures performed at low temperature (between 80 and 110 K), showed that the reflectivity of mirror surfaces basically depends on: i) the quality of thin reflecting metal layers, ii) the coating, iii) the temperature. Results show an emissivity lower than the requirement, by a factor of about 10, in the frequency range 100–380 GHz.

The emissivity was also measured indirectly in flight by the HFI, from thermal arguments: the background power in the bolometer bands, coming from the primary and secondary mirrors, was measured for each detector. Results, reported in [5] show an emissivity of about 0.07%, one order of magnitude lower than the requirement, obtained from the least squares fit of the computed in-band power from the two mirrors. Emissivity is assumed to be frequency independent. As reported in [5], these results are affected by a large uncertainty (up to 100%), especially at the two highest frequencies (545 GHz and 857 GHz), possibly due to calibration error in the bolometer plate temperature thermometer or to thermal gradients between thermometer and bolometers location (Fig. 6).

The TLT allowed to measure emissivity also in the Planck complementary frequency range covered by LFI radiometers. To first order, the mean differential power

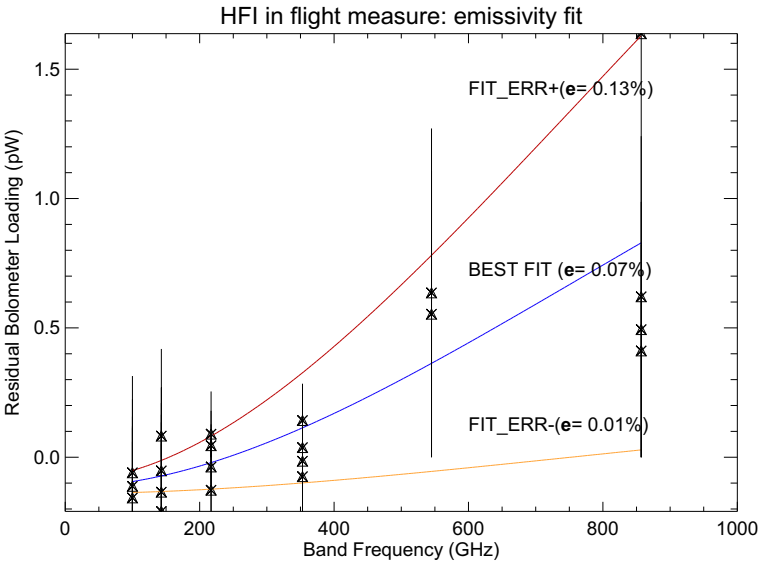


**Fig. 6** Emissivity fit calculated by HFI from thermal arguments. This plot is derived from Fig. 16 in [5]. It displays the Residual Bolometer Loading (pW) versus Frequency (GHz). All frequency channels are evenly constraining the emissivity of the mirrors (a common error on the bolometer plate temperature thermometer is considered): this leads to an estimate of 0.07 +/− 0.06% for each of the two mirrors, using a common 38K Planck Black Body law. Three cases are shown: best fit (0.07%, blue line), fit with positive error (0.07 + 0.06%, red line), fit with negative error (0.07 - 0.06%, orange line). Error bars correspond to experimental errors at each frequency for each detector. The best fit, and the two uncertainty curves, result from considering all points simultaneously

output for each of the four receiver diodes of the LFI radiometers can be written as ((1), [14]):

$$P_{\rm out}^{\rm diode} = a\, G_{\rm tot}\, k\, \beta \left[\tilde{T}_{\rm sky} + T_{\rm noise} - r\,(T_{\rm ref} + T_{\rm noise})\right], \tag{1}$$

where $G_{\rm tot}$ is the total gain, $k$ is the Boltzmann constant, $\beta$ the receiver bandwidth and $a$ is the detector constant. $\tilde{T}_{\rm sky}$ and $T_{\rm ref}$ are, respectively, the apparent average sky antenna temperature and the reference load antenna temperature at the inputs of the first hybrid; $T_{\rm noise}$ is the receiver noise temperature. $\tilde{T}_{\rm sky}$ is the apparent sky signal entering the first hybrid after the two reflections on the primary and on the secondary mirrors. The two reflections combine, attenuating the true sky signal and adding a spurious thermal signal proportional to the emissivity of the mirrors. Each term contributing to $\tilde{T}_{\rm sky}$, as detailed in the below (2) and in equations from (6) to (8), is calculated by applying a standard BB model (3); $\varepsilon_1$ and $\varepsilon_2$ is the emissivity respectively of the PR and SR.

$$\tilde{T}_{\rm sky} = (1-\varepsilon_1)(1-\varepsilon_2)T_{\rm br}^{\rm CMB} + (1-\varepsilon_2)\varepsilon_1 T_{\rm br}^{\rm PR} + \varepsilon_2 T_{\rm br}^{\rm SR} \tag{2}$$

$$T_{\rm br}^{\rm i} = \frac{h\nu}{k} \frac{1}{e^{\frac{h\nu}{kT_{\rm phys}^{\rm i}}} - 1} \tag{3}$$

Coherently, $T_{\rm ref}$ is (4):

$$T_{\rm ref} = \frac{h\nu}{k} \frac{1}{e^{\frac{h\nu}{kT_{\rm phys}^{\rm ref}}} - 1} \tag{4}$$

The gain modulation factor ((2), [14]), $r$, is defined by:

$$r = \frac{\left\langle \tilde{T}_{\rm sky} \right\rangle + \langle T_{\rm noise} \rangle}{\langle T_{\rm ref} \rangle + \langle T_{\rm noise} \rangle}, \tag{5}$$

The parameter $r$ is used to balance, in the data post processing, the temperature offset between the sky and reference load signals, minimizing the residual $1/f$ noise in the differential data stream: it is calculated each pointing period (typically lasting from $\sim 40$ to $\sim 50$ minutes, varying with the scanning strategy) from the average uncalibrated total power data.

In order to accurately characterize the telescope emissivity, a good knowledge of the following quantities is mandatory:

- PR AND SR TEMPERATURES: they affect $\tilde{T}_{\rm sky}$. To this aim, we must consider that the thermal sensors have limited resolution (about 0.2K).
- 4K REFERENCE LOAD (4KRL) STAGE THERMAL STABILITY: it affects $T_{\rm ref}$. Instabilities at 4KRL level impact on the differenced output of LFI radiometers, mimicking a change in the measured sky signal.
- LFI DETECTORS CALIBRATION CONSTANTS: they affect $G_{\rm tot}$. Any errors in the calibration constants propagate as a multiplicative error in the emissivity.
- FRONT END UNIT (FEU) THERMAL STABILITY: it affects $G_{\rm tot}$. Instabilities at FEU level impact on the gain of the front end low noise amplifiers.
- BACK END UNIT (BEU) THERMAL STABILITY: it affects $G_{\rm tot}$ and $a$. Instabilities at BEU level can either impact on the gain and bias offset of the back end low noise amplifiers or on the power suppliers of the radiometers (controlling the FEU LNAs gain), or on both.

A detailed analysis of these systematic effects is given in [13, 15]. They were all accounted for in the test preparation and execution and in the data analysis.

The total signal transmitted from PR and SR can be written as:

$$T_{\rm PR}^{\rm out} \approx (1 - \varepsilon_1) T_{\rm sky} + \varepsilon_1 T_{\rm PR} \tag{6}$$

$$T_{\rm SR}^{\rm out} \approx (1 - \varepsilon_2)[(1 - \varepsilon_1) T_{\rm sky} + \varepsilon_1 T_{\rm PR}] + \varepsilon_2 T_{\rm SR} \tag{7}$$

$$T_{\rm SR}^{\rm out} \equiv \tilde{T}_{\rm sky} \tag{8}$$

PR and SR were manufactured following a common procedure and using the same materials. For this reason, we can assume that:

$$\varepsilon_1 \approx \varepsilon_2 \sim \varepsilon \tag{9}$$

In the limit of low emissivity $\varepsilon$, the quadratic term $\varepsilon^2 \sim \varepsilon_1 \cdot \varepsilon_2$ can be neglected, reducing the above equations to a simple expression relating the antenna temperature

variation, as a function of the frequency, to the thermal excess due to the heating of the PR and SR reflectors:

$$\Delta\tilde{T}_{\rm sky} \approx \varepsilon(\Delta T_{\rm PR} + \Delta T_{\rm SR}) \tag{10}$$

$T_{\rm sky}$, $T_{\rm ref}$, $T_{\rm PR}$ and $T_{\rm SR}$ given in the equations from (1) to (10) are respectively the *brightness temperatures* of the sky signal, reference load signal, primary and secondary mirrors, calculated applying a common BB Planck Law model.

## 5 Data analysis

The differenced output from each diode of the LFI detectors was correlated to the nominal temperature changes of the primary and secondary reflectors. The temperature associated to the reflectors was the average among the sensors respectively monitoring the PR and the SR. This choice is the most conservative basing on thermal and radiometric considerations:

- Equation (10) bases on the temperature difference between the two steady states (high and low) of each mirror. The maximum discrepancy in the total $\Delta$T descending from the sensors used is 0.15 K, causing a negligible ($\leq 2\%$) uncertainty in the calculated total emissivity. The specific contributions to error budget are reported in Tables 1, 2, 3, and accounted for in the plot in Fig. 20.
- The Planck-LFI instrument has a plane of symmetry cutting in two the focal plane unit (Fig. 7), implying that the optically paired feedhorns look thermally equivalent regions of the PR and SR.
- It descends from Fig. 4 of [8] that the 10 dB footprint projected onto the primary mirror is roughly centred in a point common to all the channels while the footprint projected onto the SR is slightly offset ($\leq 200$ mm), depending on the frequency channel: comparison to Figs. 4 and 5 shows that the monitoring sensors of PR and SR are placed in positions close enough to the centres of the 10 dB contours and that the 10 dB contour is diluted over a large area of each mirror, justifying the choice to average among the temperatures of the sensors.

**Table 1** Telescope emissivity

| RCA | Emissivity | St.Dev | Sensor error |
|---|---|---|---|
| 70 GHz | 5.55E-04 | 1.19E-04 | 4.8E-06 |
| 44 GHz | 4.74E-04 | 8.74E-05 | 4.1E-06 |
| 30 GHz | 3.85E-04 | 5.54E-05 | 3.4E-06 |

Results are displayed per frequency channel together with the associated uncertainties: 'St.Dev' is the standard deviation of the emissivity of all the radiometers sharing the same frequency; 'Sensor Error' is the deviation from the calculated emissivity when the pair of sensors maximizing $\Delta T$ is considered instead of the average of the sensors, respectively of the PR and SR mirror. The 'Sensor Error' is sensibly smaller than the static variance, used as input for error bars displayed in Fig. 20

**Table 2** Telescope emissivity

| | RADIOMETER | | | |
|---|---|---|---|---|
| RCA | M | Sensor error | S | Sensor error |
| LFI18 | 5.25E-04 | 4.6E-06 | 6.19E-04 | 5.4E-06 |
| LFI19 | 6.18E-04 | 5.4E-06 | 6.48E-04 | 5.6E-06 |
| LFI20 | 5.76E-04 | 5.0E-06 | 6.87E-04 | 6.0E-06 |
| LFI21 | 5.51E-04 | 4.8E-06 | 6.15E-04 | 5.3E-06 |
| LFI22 | 5.47E-04 | 4.8E-06 | 5.51E-04 | 4.8E-06 |
| LFI23 | 2.18E-04 | 1.9E-06 | 5.11E-04 | 4.4E-06 |
| LFI24 | 3.57E-04 | 3.1E-06 | 5.32E-04 | 4.6E-06 |
| LFI25 | 4.79E-04 | 4.2E-06 | 4.91E-04 | 4.3E-06 |
| LFI26 | 5.93E-04 | 5.2E-06 | 3.93E-04 | 3.4E-06 |
| LFI27 | 3.03E-04 | 2.6E-06 | 3.99E-04 | 3.5E-06 |
| LFI28 | 4.20E-04 | 3.6E-06 | 4.18E-04 | 3.6E-06 |

Results are displayed per radiometer. M and S correspond to MAIN and SIDE radiometers [4] (Fig. 17). Each value reported for M and S is obtained by averaging the two paired detectors of the same radiometer. For each value, the accuracy of the measurement is provided: it estimates the maximum deviation from the emissivity calculated using the average of all the available sensors placed on PR and SR mirror, corresponding to the use of the two PR and SR sensors maximizing $\Delta$T

Data were calibrated averaging the nominal gains calculated during one day in the late routine phase (day 1480 after launch) before the TLT. The calibration constants used are reported in the Appendix (Table 4).

The effect of the signal fluctuations induced by the dipole modulation, caused by the Planck Telescope spinning, was also taken into account. Results, after the dipole contribution removal, differ only negligibly from those before correction.

The results were also corrected for the radiometer susceptibility to the temperature changes of: the front end unit (FEU), the back end unit (BEU) and the 4K stage

**Table 3** Telescope emissivity

| RCA | Emissivity |
|---|---|
| LFI18-LFI23 | 4.68E-04 |
| LFI19-LFI22 | 5.91E-04 |
| LFI20-LFI21 | 6.07E-04 |
| LFI25-LFI26 | 4.89E-04 |
| LFI27-LFI28 | 3.85E-04 |

Results are displayed per optically paired channels, corresponding to feedhorns that are placed symmetrically w.r.t the plane of symmetry of the telescope. LFI24 is not reported because it is not paired to any other channels (it is placed in the plane of symmetry of the telescope). MAIN and SIDE radiometers data have been averaged [4]

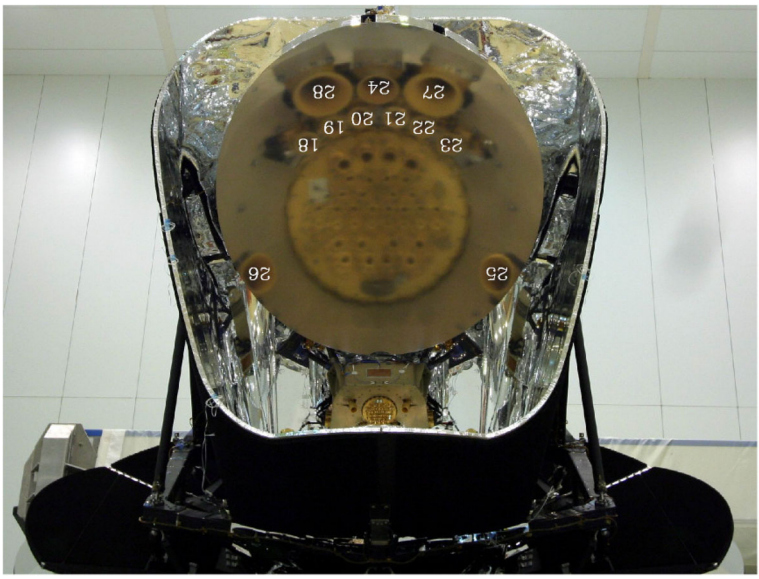


**Fig. 7** The HFI and LFI feed horn images reflected in the primary mirror of the Planck telescope during the PLANCK Pre-Launch tests performed in the clean room of the *Centre Spatial Guyanais* (CSG) at Kourou, French Guiana. The LFI channels are numbered as it follows: from 18 to 23 (70 GHz), from 24 to 26 (44 GHz) , from 27 to 28 (30 GHz). Channels symmetric w.r.t. the plane of symmetry of the Planck satellite are said '*optically coupled*'. Channel LFI24 is centred in the plane of symmetry and is not coupled to any of the two other 44 GHz channels. ©ESA/Thales

(4KRL). Also with respect to these systematic effects, differences were negligible, because of the high thermal stability of the LFI during the TLT test.

The LFI thermal behaviour is shown in the following figures. The peak to peak variations are:

- lower than 0.05 K in the FEU (Fig. 8);
- at the level of sensors resolution in the BEU (Figs. 9 and 10 show quantized signals);
- lower than 4 mK in the 4K Reference Load Unit (Fig. 11);

All the above effects do not show any correlations with the temperature changes in the PR and SR. Reference values for the thermal susceptibilities are those from [13].

The temperature variation of primary and secondary reflectors, averaged over the sensors monitoring each reflector, is displayed in Fig. 12 and in Fig. 13. The relevant quantity is not the absolute temperature, but instead the thermal change due to reflector heating. The emissivity was calculated in thermal steady-state conditions of the PR and SR (by comparing two time windows, before and after the thermal transient): the same analysis was repeated in transient conditions, resulting in differences of a few percent. The steady state analysis was considered more reliable, because it cancels the possible phase error due to the thermal inertia of the telescope and mitigates the thermal gradients over the PR and the SR surface during the heating phase.

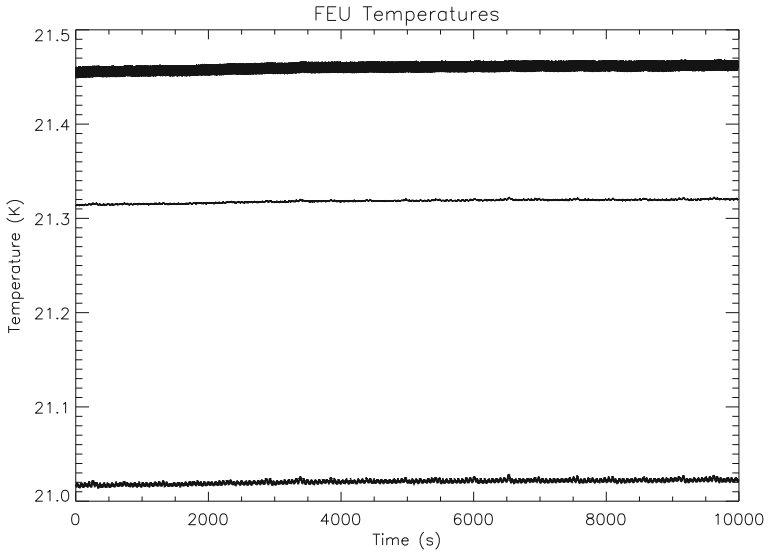


**Fig. 8** Front end unit sensors positioned near feedhorn LFI28, LFI25, LFI26. They correspond to the three LFI Q band channels [4]

The effect on the radiometers caused by the heating of PR and SR is shown for one detector of the three channels `LFI18`, `LFI25`, `LFI28`, representative of the full LFI frequency range (70 GHz, 44 GHz and 30 GHz respectively), in Figs. 14, 15 and 16: in order to simplify the visualization, data have been rebinned. For each detector, the radiometric output expected by model is superimposed. The detector Gain and

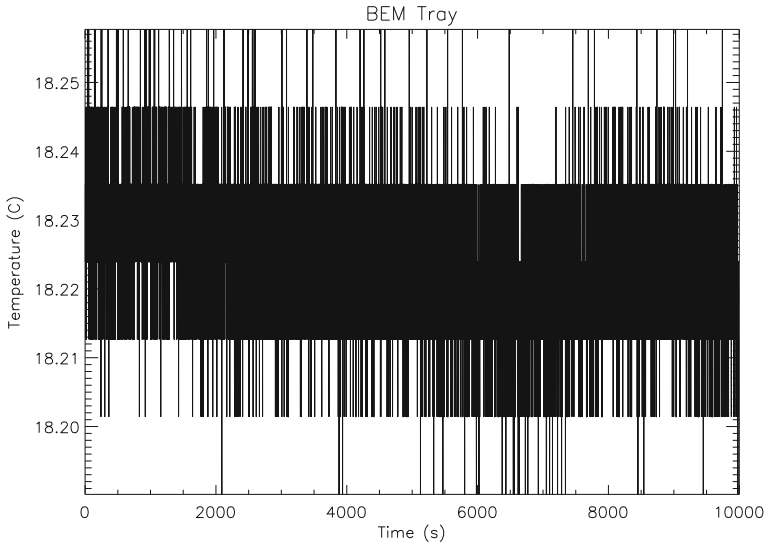


**Fig. 9** Back end unit sensors positioned on BEM tray ([4])

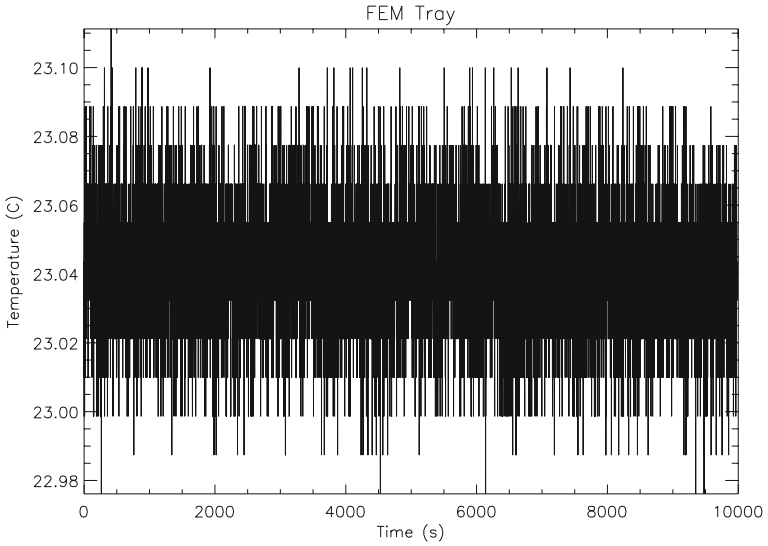


**Fig. 10** Back End Unit sensors positioned on FEM tray [4]

the emissivity (averaged over all the channels at that specific frequency) are input of the model; the residual, at some extent, represents the deviation of the individual detectors from the model based on a unique emissivity as a function of the frequency only. The differential nature of the LFI radiometers and their high sensitivity [9] make it possible to identify clearly the sky temperature excess due to reflectors heating.

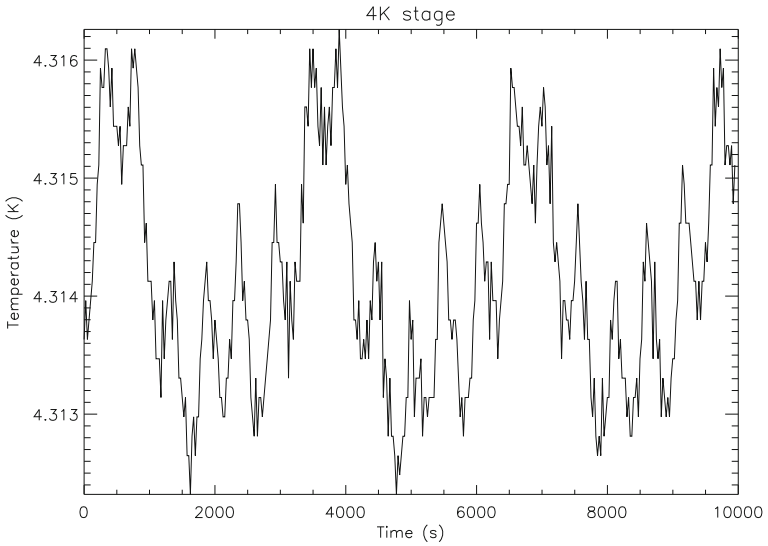


**Fig. 11** 4K stage temperature

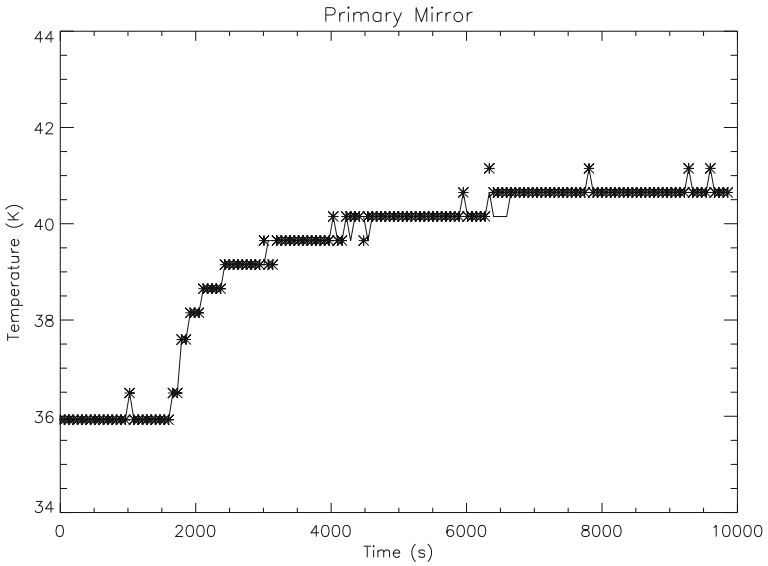


**Fig. 12** Primary reflector temperature averaged between three PR sensors

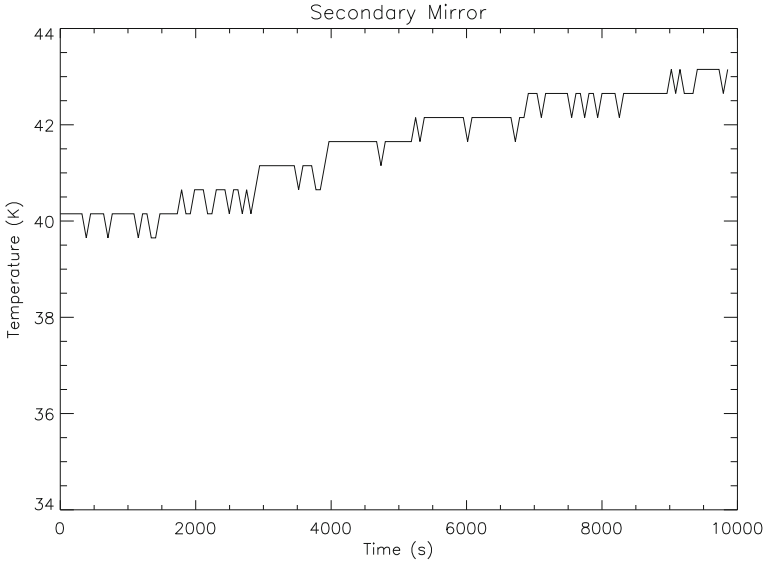


**Fig. 13** Secondary reflector temperature averaged between three SR sensors

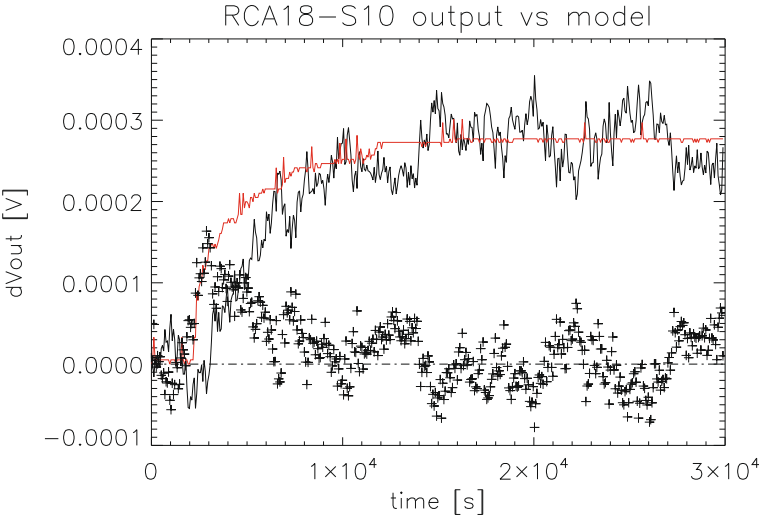


**Fig. 14** Differenced output change in the 70 GHz channel LFI-1810 (S) caused by telescope heating during TLT: smoothed data (black solid curve) are compared to radiometric output variation modelled (red curve). The residual, resulting from the difference between measured and modelled data, is also shown (black crosses) together with the 0V reference level. Residual, especially in steady state conditions, is close to 0

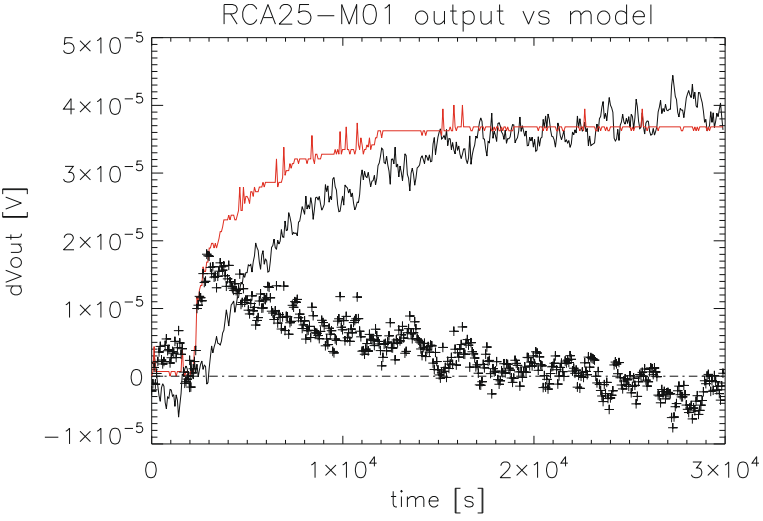


**Fig. 15** Differenced output change in the 44 GHz channel LFI-2501 (M) caused by telescope heating during TLT: smoothed data (black solid curve) are compared to radiometric output variation modelled (red curve). The residual, resulting from the difference between measured and modelled data, is also shown (black crosses) together with the 0V reference level. Residual, especially in steady state conditions, is close to 0

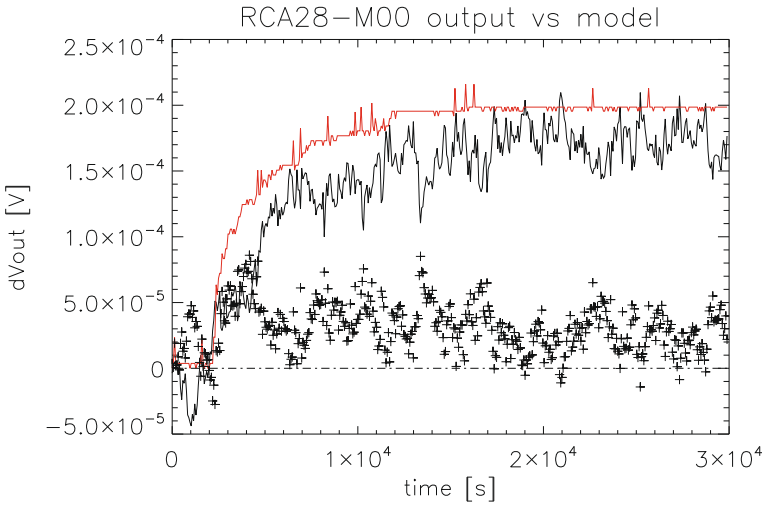


**Fig. 16** Differenced output change in the 30 GHz channel LFI-2800 (M) caused by telescope heating during TLT: smoothed data (black solid curve) are compared to radiometric output variation modelled (red curve). The residual, resulting from the difference between measured and modelled data, is also shown (black crosses) together with the 0V reference level. Residual, especially in steady state conditions, is close to 0

## 6 Results

Results are presented for each frequency channel in Table 1.

Results are presented per radiometer (`Main`, `Side`) in Table 2, showing for each channel the emissivity corresponding to the measured apparent sky temperature excess caused by telescope heating. Differenced outputs from coupled diodes are linearly combined as described in [17]. The detailed scheme of a LFI radiometer is shown in Fig. 17 [4].

`MAIN` and `SIDE` radiometers of the channel `LFI23` show an emissivity quite different from each other. This is caused by the detector LFI-2300, which appeared quite insensitive to the test, showing a flat-like response, while its paired channel LFI-2301 responded instead as expected. Although this detector could be treated as an outlier, discarding its results from the general analysis, we preferred to include it since we did not find any technical reasons suggesting to discard data for this channel; this just translates into a larger standard deviation.

A different way to combine results is shown in Table 3, where the measured excess is presented averaging over the LFI optically paired channels: this approach is aimed at accounting for a possible inhomogeneity in the temperature of the reflectors. The channels have been paired basing on the scheme reported in Table 3 (channel `LFI24` is not considered, as it is odd in that it is not paired to any other channels).

The telescope emissivity, per frequency channels (values from Table 1), was compared to the values reported in Appendix of [1], where the measured dependence of the Reflection Loss (1-R) of a sample of Planck reflector material is shown at 110 K, as a function of frequency, in the range 100–380 GHz.

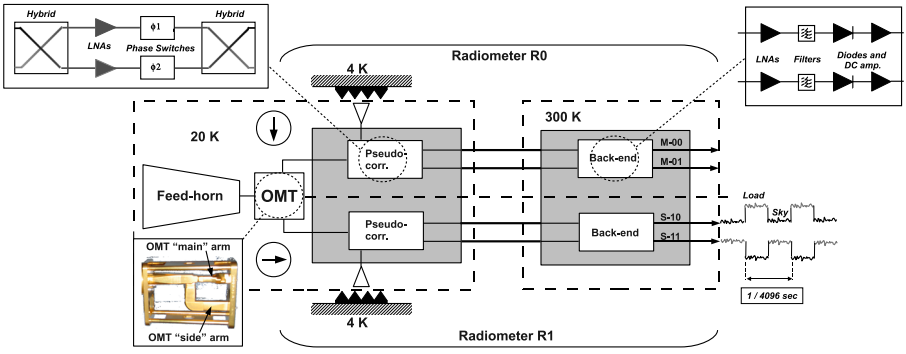


**Fig. 17** A complete RCA from feed-horn to analogue voltage output. The insets show the OMT, the details of the 20 K pseudo-correlator and of the back-end radio-frequency amplification, lowpass filtering, detection and DC amplification. The two perpendicular linear polarisation components split by the OMT propagate through two independent pseudo-correlation differential radiometers, labelled as `M` or `S` depending on the arm of the OMT they are connected to ("Main" or "Side"). In each radiometer the sky signal coming from the OMT output is continuously compared with a stable 4 K blackbody reference load mounted on the external shield of the HFI 4 K box [6]. After being summed by a first hybrid coupler, shown in the upper-left inset, the two signals are amplified by $\sim 30$ dB. The four outputs of the two differential radiometers are named with the sequence: `M1`, `M2` (radiometer `MAIN`) and `S1`, `S2` (radiometer `SIDE`)

Differences in the Reflection Loss are expected between *in-flight* tests (TLT) and *on-ground* tests [1], due to the different temperature of the telescope: the largest differences are expected at high frequency [18]. This frequency dependency allowed to superpose results from the TLT test, obtained at 40K in the range 27 GHz - 77 GHz, to results from Fig. B1 - right - in [1], obtained at 110 K and at 296 K in the range 100 GHz - 380 GHz. Comparison is shown in Fig. 18.

### High Frequency Data Extrapolation to 40 K

A more accurate comparison among the data sets, at different temperatures, is obtained by extrapolating down to 40K the high frequency data (100 GHz - 380 GHz) measured at 110 K.

The temperature dependence of the Reflection Loss was modelled basing on the experimental evidences described in [19], considering the case of mirrors of highly pure aluminum (99.99% Al) at the fixed frequency f = 150 GHz. At cryogenic temperature, below 150K, experimental results deviate (exceeding by about 65%) from the purely theoretical model, suggesting an almost linear decrement of the Reflection Loss down to 40K (plot 10 in [19]). This supports our choice to linearly fit ($R \geq 0.99$) the Reflection Loss in the range 110 K : 300 K and to extrapolate results down to 40 K. (Fig. 19; error bars for data at HFI frequencies, at 296K and 110K, were not available).

The measured emissivity at LFI frequencies - at 40 K - is, as expected, lower than the emissivity measured at 110 K, at the HFI frequencies, and slightly higher than extrapolated data.

Reflection Loss, at cryogenic temperature, depends on the purity level of the material; in addition, in the specific case of a Space Telescope, cleanliness of the mirrors

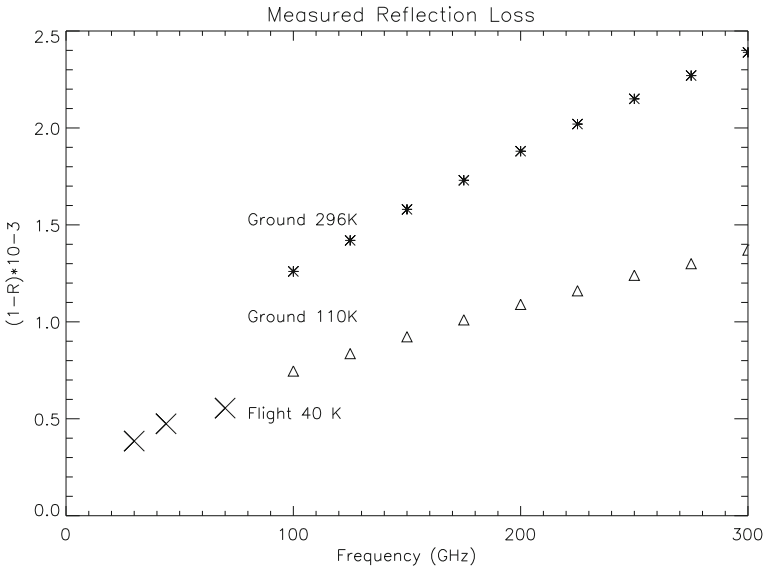


**Fig. 18** In-flight Reflection Loss at 40K compared to data from [1]. They are respectively shown: experimental data from ground test @296 K (asterisk); experimental data from ground test @110 K; experimental data from LFI in-Flight measurement (this work) at 40K (cross)

at the end of mission and aging can play a crucial role. Despite everything, deviations of measured from extrapolated data can be considered negligible, as they are well within the error bars of the in-flight measurement.

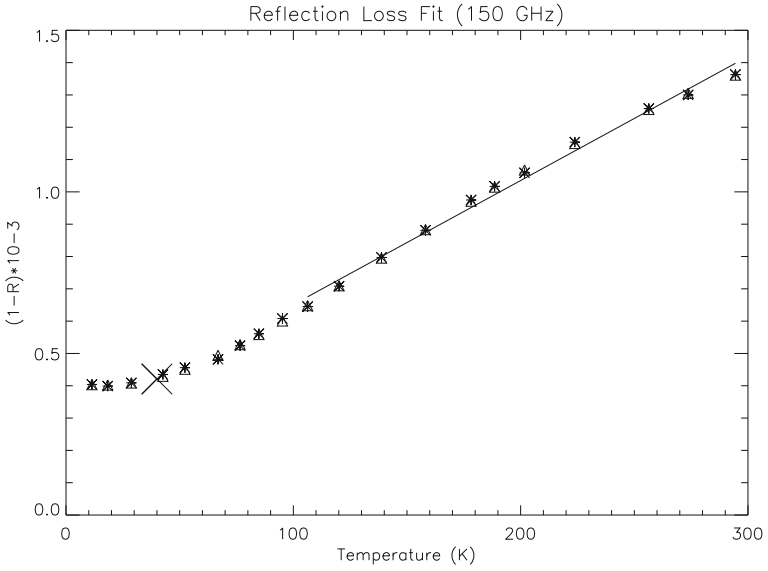


**Fig. 19** Reflection Loss at from data in [19], at 150 GHz. Stars: experimental data. Triangles: forth order polynomial fit; solid line: linear fit in the range [110 K : 296 K]. Cross: extrapolation down to 40 K

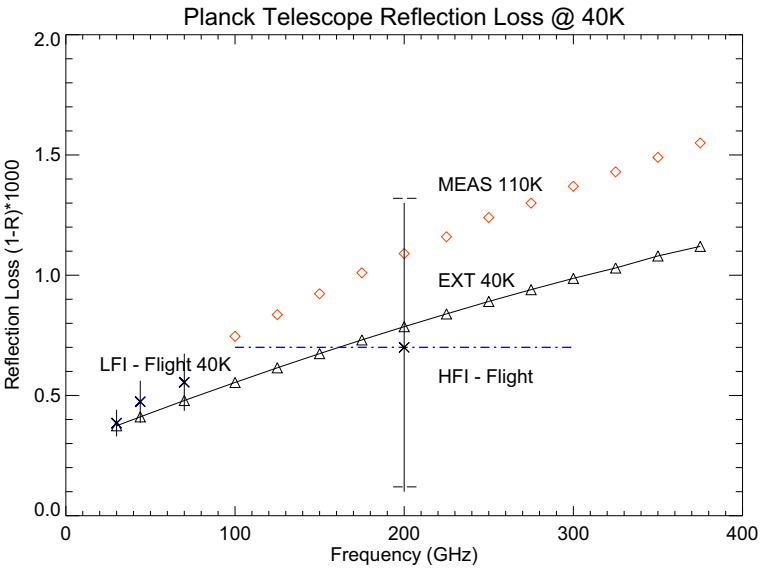


**Fig. 20** Telescope Reflection Loss. Reflection Loss data are multiplied by a factor of 1000. Results from TLT test, at LFI frequencies are compared to the following data sets: (i) data @110K from Fig.B1 -right in [1] (MEAS 110K), red diamonds; (ii) data extrapolated in temperature down to 40K and in frequency down to LFI frequencies (EXT 40K), solid line with triangles; (iii) indirect *in-flight* measure by HFI from thermal arguments (reported in [5]: HFI-FLIGHT), blue dashed-dot line: the behaviour is flat in frequency. Error bars relative to flight measures are reported. At the LFI frequencies, error bars are prudentially defined as the statistic variance from Table 1; at the HFI frequencies, error bars were selected again with a prudential approach: they correspond to the uncertainty of the emissivity best fit in Fig. 6

Results confirm the goodness of this approach and the quality of the Planck telescope in space (Fig. 20).

## 7 Conclusions

The End of Life (EOL) phase, before Planck satellite de-orbiting, represented a very useful step in completing the characterization of several instrumental properties measured before launch or during the early phases of the mission (CPV).

The telescope total emissivity was measured only indirectly (Reflection Loss tests), on test samples of the Herschel telescope first, on samples of the Planck telescope finally. Until EOL, emissivity was measured only in a reduced frequency range covered by HFI (100–380 GHz), keeping the samples at a temperature (110 K) higher than the in-flight nominal temperature of the telescope (around 40 K).

The presence of de-contamination heaters and temperature sensors on the primary and secondary reflectors permitted a dedicated measurement of the telescope emissivity at mission completion. The high sensitivity of the LFI radiometers, together with the optimal knowledge of LFI systematic effects, permitted to derive the telescope emissivity from the thermal excess measured by the LFI radiometers.

The emissivity measured is consistent with the *on ground* Reflection Loss measured in the range 100–380 GHz, extrapolated to the LFI frequencies. Slight deviations from the extrapolated curve are consistent with the improvements expected from the lower telescope temperature in flight. Extrapolation to 40K of '*on ground*' reflection Loss measured at higher temperatures showed that the telescope performance was not degraded at EOL w.r.t. BOL, and that the emissivity was about one order of magnitude better than the mission requirement.

The measure of success of future CMB experiments is how we cope with the knowledge of the systematic effects. Telescope emissivity can represent a large source of systematic uncertainties, since bigger and bigger mirrors will be required to feed thousands of receivers, needed to meet the ambitious requirements of next CMB experiments. This method could be hence usefully implemented for future space experiment, at mm and sub-mm wavelengths, to finely characterize the telescope emissivity during the mission, in nominal conditions, provided that a dedicated thermal control system, based on control loop heaters and on a network of high resolution thermometers, is present.

**Acknowledgements** The Planck Collaboration acknowledges the support of: ESA; CNES, and CNRS/INSU-IN2P3-INP (France); ASI, CNR, and INAF (Italy); NASA and DoE (USA); STFC and UKSA (UK); CSIC, MICINN, and JA (Spain); Tekes, AoF, and CSC (Finland); DLR and MPG (Germany); CSA (Canada); DTU Space (Denmark); SER/SSO (Switzerland); RCN (Norway); SFI (Ireland); FCT/MCTES (Portugal); ERC and PRACE (EU). A description of the Planck Collaboration and a list of its members, indicating which technical or scientific activities they have been involved in, can be found at URL: http://www.cosmos.esa.int/web/planck/planck-collaboration.

The Planck LFI project (including instrument development and operation, data processing and scientific analysis) is developed by an international consortium led by Italy and involving Canada, Finland, Germany, Norway, Spain, Switzerland, UK, and USA. The Italian contribution is funded by the Italian Space Agency (ASI) and INAF.

We want to give special thanks to the Planck Mission Operations Center (MOC) for the professionality and helpfulness shown during the whole Planck mission and, with respect to this work, during the LFI EOL Test Campaign.

## Appendix

**Table 4** Calibration constants (K/V)

| | RADIOMETER | |
|---|---|---|
| RCA | M (K/V) | S (K/V) |
| LFI18 | 14.2561 | 21.6802 |
| LFI19 | 26.6958 | 41.7731 |
| LFI20 | 25.0797 | 30.4108 |
| LFI21 | 44.2530 | 41.5908 |
| LFI22 | 62.7823 | 60.7783 |
| LFI23 | 34.7458 | 51.4989 |
| LFI24 | 287.7942 | 178.8558 |
| LFI25 | 126.3679 | 126.5682 |
| LFI26 | 170.7176 | 144.4097 |
| LFI27 | 12.7991 | 15.2754 |
| LFI28 | 15.8118 | 19.2263 |

Results are displayed per radiometer. M and S correspond to MAIN and SIDE radiometers

## References


1. Tauber, J.A., et al.: Planck pre-launch status: the planck mission. A&A **520**, A1 (2010)
2. Planck Collaboration I. 2011, A&A, 536, A1
3. Lamarre, J.M., et al.: Planck pre-launch status: The HFI instrument, from specification to actual performance. A&A **520**, A9 (2010)
4. Bersanelli, M., et al.: Planck pre-launch status: design and description of the low frequency instrument. A&A **520**, A4 (2010)
5. The Planck Collaboration: Planck early results. III. The thermal performance of Planck. A&A **536**, A2 (2011)
6. Valenziano, L., et al.: Planck-LFI: design and performance of the 4 Kelvin reference load unit. JINST **4**, T12006 (2009)
7. Gregorio, A., et al.: In-flight calibration and verification of the Planck-LFI instrument. JINST **8**, T07001 (2013)
8. Sandri, M., et al.: Planck pre-launch status: Low Frequency Instrument optics. A&A **520**, A7 (2010)
9. Mennella, A., et al.: Planck early results. III. First assessment of the Low Frequency Instrument in-flight performance. A&A **536**, A3 (2011)
10. Terenzi, L., et al.: Thermal susceptibility of the planck-LFI receivers. JINST **12**, T12012 (2009)
11. Cuttaia, F., et al.: Planck-LFI radiometers tuning. JINST **12**, T12013 (2009)
12. Tauber, J.A., et al.: Planck pre-launch status: the optical system. A&A **520**, A2 (2010)
13. The Planck Collaboration: Planck 2013 results. III. LFI systematic uncertainties. A&A **571**, A3 (2014)
14. Mennella, A., et al.: Planck early results. III. First assessment of the Low Frequency Instrument in-flight performance. A&A **536**, A3 (2011)
15. The Planck Collaboration: Planck 2015 results. III. LFI Systematic uncertainties, A&A submitted, arXiv:1507.08853 (2015)
16. Fischer, J., Klaassen, T., Hovenier, N., et al.: Appl. Opt. **43**, 3765 (2005)
17. The Planck Collaboration: Planck 2013 results. II. Low Frequency Instrument data processing. A&A **571**, AA2 (2014)
18. Parshin, V., van der Klooster, C.: 30th ESA Antenna Workshop (2008)
19. Serov, E.A., Parshin, V., Bubnov, G.M.: Reflectivity of metals in the millimeter wavelength range at cryogenic temperatures. IEEE Transactions Microwave THEORY Techniques, vol. 64, no. 11 (2016)
20. Stute, T.: The telescope reflectors for the ESA mission planck. Presentation at 28th ESA Antenna Workshop ESA/ESTEC Noordwijk, 02 June (2005)
21. Stute, T.: The Planck telescope reflectors. Proc. SPIE 5495. Astronomical Structures and Mechanisms Technology, 1 (September 29). https://doi.org/10.1117/12.549268 (2004)